Jpn. J. Appl. Phys. Vol. 35 (1996) pp. 4654–4659
Part 1, No. 9A, September 1996

Evaluation of Coupling Coefficients for Laterally-Coupled Distributed Feedback Lasers

Woo-Young CHOI*, Jerry C. CHEN[1] and Clifton G. FONSTAD[1]

Department of Electronic Engineering, College of Engineering, Yonsei University
134 Shinchon, Seo-dae-mun, Seoul 120-749 , Korea
[1]*Department of Electrical Engineering and Computer Science, Massachusetts Institute of Technology, Cambridge, MA 02139, USA*

(Received February 19, 1996; accepted for publication July 15, 1996)

Dependence of coupling coefficient, κ, on laterally-coupled distributed feedback (LC-DFB) laser structure is investigated. In LC-DFB lasers, gratings are fabricated on and around the ridge after ridge-waveguide formation and, thus, neither epitaxial regrowth nor growth on corrugated substrates is required. For κ calculation, coupled-mode theory is used with the two-dimensional field intensity calculated using the imaginary-distance beam propagation method. Comparisons are made for LC-DFB lasers with different layer, ridge and grating structures and parameters that affect κ are identified. In addition, it is shown that LC-DFB structure is less sensitive to processing variations and, thus, more manufacturable than a conventional buried heterostructure DFB structure.

KEYWORDS: DFB laser, laterally-coupled DFB, coupling coefficient, BPM, gratings

1. Introduction

Recently there is a growing interest in laterally-coupled distributed feedback (LC-DFB) lasers.[1-3] In an LC-DFB laser, gratings are fabricated, as schematically shown in Fig. 1(a), on and around the ridge of a conventional ridge-waveguide laser and coupling between gratings and lateral evanescent fields provides the necessary feedback. As gratings are fabricated after the formation of the ridge, LC-DFB lasers do not require epitaxial regrowth nor growth on corrugated substrates. Although such processes are routinely performed for fabricating conventional DFB lasers, they are still hard-to-control processes and often a yield- or reliability-limiting step. Thus, LC-DFB lasers are expected to have a great advantage of simpler fabrication. Even if the performance of LC-DFB lasers is not likely to match that of conventional DFB lasers, this advantage of simpler fabrication and the consequential cost reduction make LC-DFB lasers a promising candidate for applications in which cost consideration is an important factor as in optical local access networks. Furthermore, LC-DFB lasers are expected to find applications for lasers based on materials for which epitaxial regrowth is technically very challenging.

There have been several attempts to realize LC-DFB lasers. Martin *et al.* fabricated LC-DFB lasers using electron-beam lithography and demonstrated CW single-mode operation of InGaAs/GaAs/AlGaAs lasers.[3] Wong *et al.* fabricated grating structures for InP-based LC-DFB lasers using X-ray lithography which, with large depth-of-focus and the absence of a proximity effect, is expected to be more suitable for making gratings over the ridge than electron-beam lithography.[2] Although these studies have demonstrated the realization of grating structures that provide sufficient κ values, there have been no detailed studies that investigate κ dependence on LC-DFB laser structures. As reliable and consistent realization of required κ values is the key factor for achieving low-cost LC-DFB lasers, theoretical investigations of κ dependence on possible structural as well as processing variations should be of great importance. In this paper, results of such investigations are presented that have been performed as a first step toward realizing optimal InP-based 1.55 μm LC-DFB lasers.

*Corresponding author

2. Method of κ Calculation

Figure 1(a) schematically shows the LC-DFB structure in which gratings are etched on the channel next to the ridge as well as on top of the ridge side-walls. For simplicity in calculation, the contact layer of lower bandgap material and metal pads are not considered since their influence on κ is expected to be very small. Coupled-mode theory is used for κ calculation.[4] According to coupled-

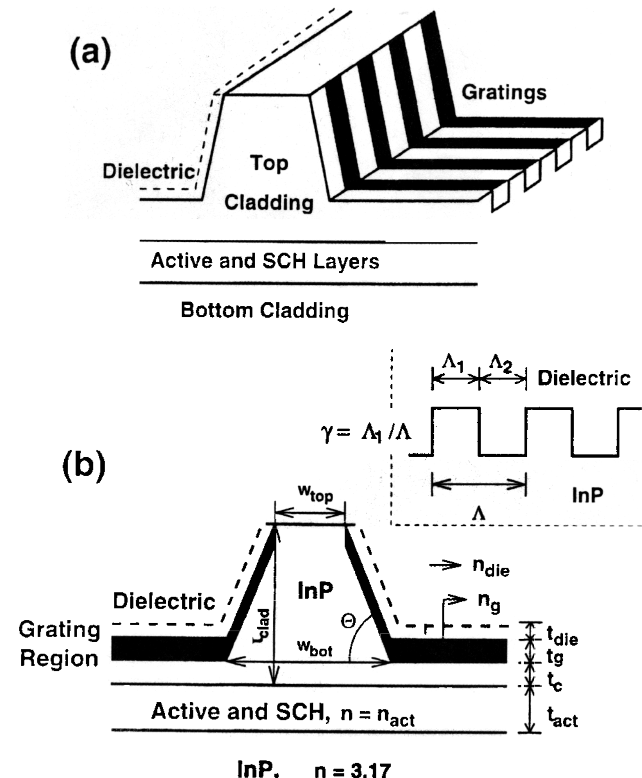

Fig. 1. (a) A schematic drawing of LC-DFB laser whose κ value is investigated. (b) A generic waveguide structure with definitions for various parameters used.

mode theory, the magnitude of κ for rectangular-shape gratings is given as,[5]

$$|\kappa| = \frac{(n_2^2 - n_1^2)}{n_{\rm eff}\lambda}\frac{\sin(\pi m\gamma)}{m}\Gamma, \quad (1)$$

where n_1 and n_2 are refractive indices of materials above and below the gratings; $n_{\rm eff}$ is the effective mode index of the waveguide; λ is the wavelength of interest; m is the grating order; γ is the grating duty cycle defined as Λ_1/Λ where Λ_1 and Λ are defined in the inset of Fig. 1(b); Γ is the field overlap integral with the grating region, or the fraction of the unperturbed mode intensity residing inside the grating region. Although the perturbational approach of coupled-mode theory may not be adequate for κ calculation if gratings are very deep in the conventional DFB structures,[6] it is not the case here since the amount of perturbation even with very deep gratings in the present investigation is very small as can be seen from the small κ values calculated in later sections.

In order to determine κ, numerical values of $n_{\rm eff}$ and Γ are required for a given LC-DFB structure. Both of these are determined from the fundamental mode profile calculated numerically with the imaginary-distance beam propagation method (IDBPM). In IDBPM, beam propagation is made along the imaginary axis where only eigen modes of the given waveguide can survive.[7] As the required propagation step can be large, IDBPM can produce accurate solutions quite efficiently. The details of our IDBPM implementation and its accuracy can be found elsewhere.[8]

Figure 1(b) shows a generic waveguide structure used for the field profile calculation by the IDBPM. Here, the grating region is represented by a homogeneous layer with a weighed average dielectric constant between the materials above (dielectric) and below (InP) the gratings,[9] or in terms of refractive indices,

$$n_{\rm g}^2 = \frac{\Lambda_1}{\Lambda}n_{\rm die}^2 + \frac{\Lambda_2}{\Lambda}n_{\rm InP}^2. \quad (2)$$

For simplicity in numerical calculations and in order to generalize many different active and SCH layer structures possible, the active and SCH layers are lumped together into one homogeneous layer with an effective refractive index, $n_{\rm act}$, and thickness, $t_{\rm act}$. $n_{\rm act}$ is determined in a similar manner to $n_{\rm g}$, or

$$n_{\rm act}^2 = \frac{\sum_i t_i n_i^2}{t_{\rm act}}, \quad (3)$$

where t_i and n_i correspond to thickness and refractive index in each layer making up the active and SCH layers, and $t_{\rm act}$ is the total thickness or $\sum_i t_i$. This type of approximation is frequently used for MQW waveguides and the error in the propagation constant due to the approximation is known to be very small.[10] This approximation is not expected to cause any significant errors in our determination of κ, either, since we are only concerned with the field intensity in the grating region where the very details of the active and SCH layers do not matter too much as long as they are properly accounted for in an effective manner.

Although some of the waveguide structures considered in this paper can support higher lateral modes, only the fundamental lateral mode is used for κ calculations since it is most relevant for practical laser applications. Clearly, waveguides with multiple lateral modes are not desirable and they are considered in this paper only for comparison purpose. In addition, TE polarization, wavelength of 1.55 μm, and the first order grating ($m = 1$ in eq. (1)) are used for κ calculations. The grid sizes used for IDBPM calculations are 0.1 and 0.02 μm within the area of 10 μm by 2.5 μm for x and y axes, respectively. The definition for x and y axes can be found in Fig. 2. Under these conditions, the calculation takes a few minutes on a RS6000 workstation before the fundamental eigen mode profile and $n_{\rm eff}$ converge. Figure 2 shows a result of such IDBPM calculation in a contour plot of the field intensity along with the values of refractive indices used.

3. Dependence of κ on Active and SCH Layer Structures

InP-based lasers can employ many different active and SCH layer structures. A double-heterostructure (DH) laser, for example, can have a bulk InGaAsP active layer without any SCH layers, whereas a strained single QW laser has much thicker SCH layers than the active region. Since the different transverse field profiles resulting from such differences affect κ, it is necessary to understand the influence of the active and SCH layer structures on κ before other factors are considered. In order to cover the wide ranges of $n_{\rm act}$ and $t_{\rm act}$ produced by eq. (3) for different active and SCH layer structures, three sets of $n_{\rm act}$ and $t_{\rm act}$ are determined for laser structures found in the literature and their κ values in identical ridge-waveguide structures are calculated and compared: $n_{\rm act} = 3.57$ and $t_{\rm act} = 0.2\,\mu$m representing a typical DH laser with a bulk InGaAsP active layer of $\lambda = 1.55\,\mu$m, $n_{\rm act} = 3.45$ and $t_{\rm act} = 0.31\,\mu$m obtained from a strained MQW (five wells) laser structure studied by Sato *et al.*,[11] and $n_{\rm act} = 3.31$ and $t_{\rm act} = 0.21\,\mu$m obtained from a strained single QW laser structure reported by Tsang *et al.*[12] Refractive indices for given InGaAsP compositions are obtained from the work of Henry *et*

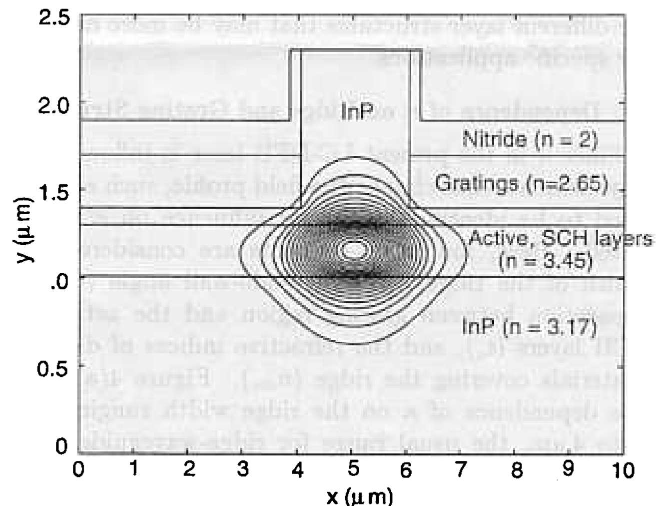

Fig. 2. An example of a contour plot for field intensity obtained with IDBPM.

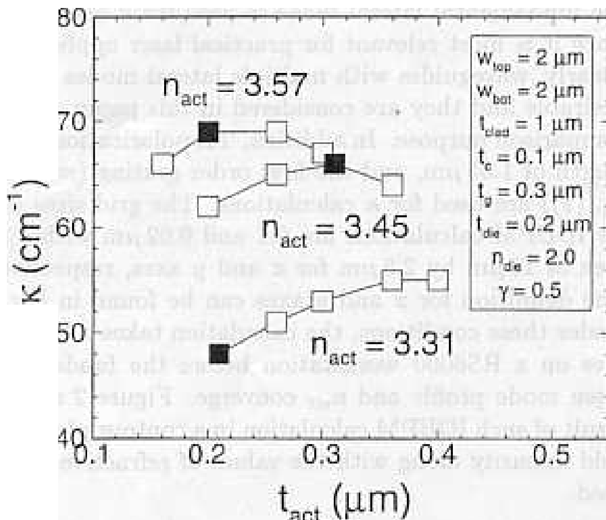

Fig. 3. κ dependence on various combinations of n_{act} and t_{act}.

al.[13] For QWs, the refractive index of bulk material is used that has the same band-gap as the ground state electron-to-heavy-hole transition energy in the well.

The filled squares in Fig. 3 show the calculated κ values for above three sets within a LC-DFB structure described by the parameters shown in the inset. Clearly, κ depends on n_{act} and t_{act}. In order to better understand this dependence, κ values are calculated for some additional values of t_{act} for each n_{act} and are shown as empty squares in Fig. 3. As shown in the figure, higher n_{act} gives larger κ at fixed t_{act}. Also κ peaks at a certain value of t_{act} with given n_{act}, where the peak position increases with decreasing n_{act}. This dependence is entirely due to the different overlap integral, Γ, resulting from the different field profiles with different values of n_{act} and t_{act}. Since the variation in κ for ranges of n_{act} and t_{act} of interest is not too great and the number of parameters involved needs to be reduced, we use $n_{act} = 3.45$ and $t_{act} = 0.3\,\mu$m for the subsequent investigations. In other words, all our investigation in the following sections are based on the epitaxial layer structure used in the work of Sato *et al.*[11] This is only a choice of convenience and all the observations should hold qualitatively for different layer structures that may be more desirable for specific applications.

4. Dependence of κ on Ridge and Grating Structures

Since κ in the present LC-DFB laser is influenced by any elements that change the field profile, such elements need to be identified and their influence on κ investigated. Here, four such elements are considered first: width of the ridge, the ridge side-wall angle (Θ), the separation between grating region and the active and SCH layers (t_c), and the refractive indices of dielectric materials covering the ridge (n_{die}). Figure 4(a) shows the dependence of κ on the ridge width ranging from 2 to 4 μm, the usual range for ridge-waveguide lasers. It shows that a narrower ridge width gives larger κ, an expected result since a narrower ridge provides less lateral optical confinement and, hence, more field leaking out to the grating region. Furthermore, the sensitivity

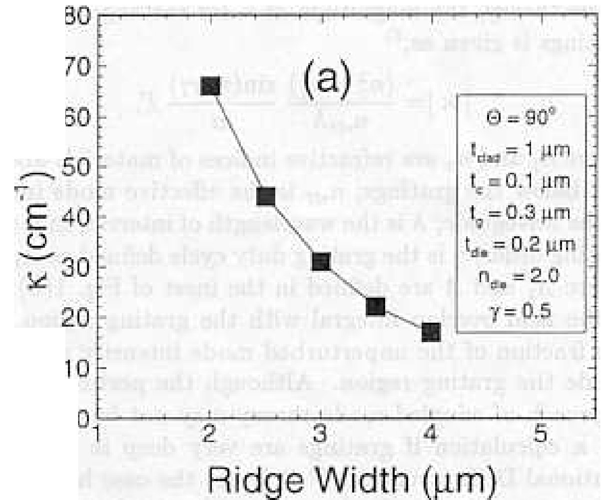

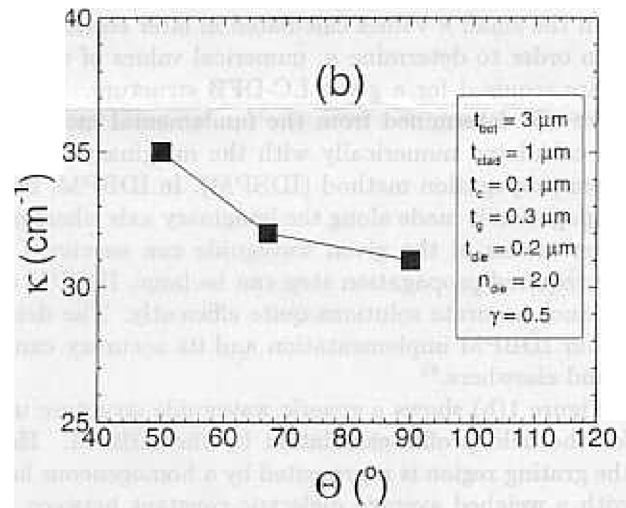

Fig. 4. κ dependence on (a) ridge width, and (b) side-wall angle

of κ to the ridge width variation is higher for narrower ridges. This implies that LC-DFB lasers with extremely small ridge widths are not desirable since they may suffer from a severe fluctuation of κ. In fact, the high κ value obtained for very narrow ridges is not optimal for actual device applications, either, since a κL product (L is the laser cavity length) of only about 1.25 is desirable.[14] If κL is too high, spatial hole burning reduces the gain margin against undesired side modes; if κL is too low, distributed feedback is insufficient. κL of 1.25 corresponds to κ of 25 cm^{-1} for a typical cavity length of 500 μm and, thus, if other parameters are kept the same, a device with a 3-μm-wide ridge is more desirable than 2 μm as far as κ is concerned.

For the investigation of Θ dependence, the bottom width of the ridge, w_{bot}, is kept at 3 μm, and the top width, w_{top}, is reduced in order to distinguish the influence of Θ from that of the ridge width investigated above. Under this condition, Fig. 4(b) shows that Θ does not greatly affect κ. This is because the field decays relatively quickly in the top cladding and decreasing the top ridge width does not greatly affect the overall field profile.

Figures 5(a) and 5(b) show the dependence of κ on

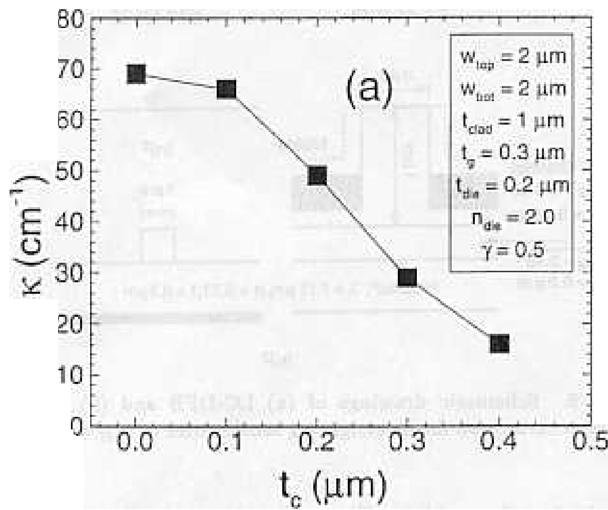

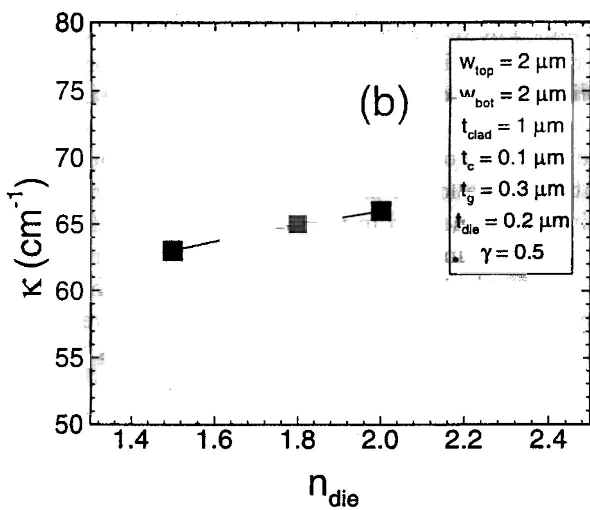

Fig. 5. κ dependence on (a) t_c, the separation between grating region and active and SCH layers, and (b) $n_{\rm die}$, the refractive index of dielectric material covering the ridge.

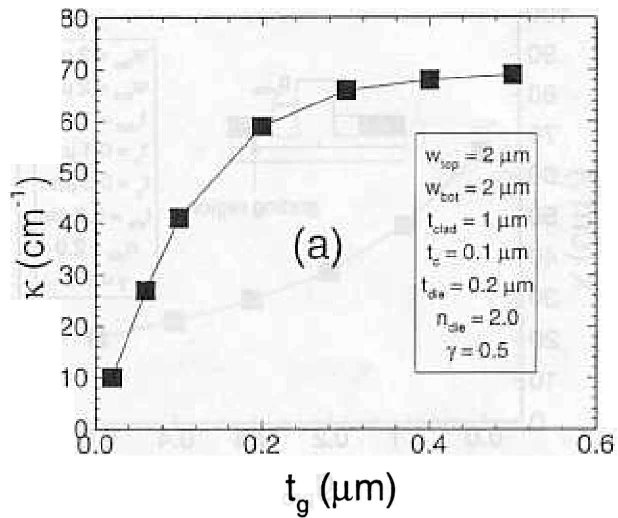

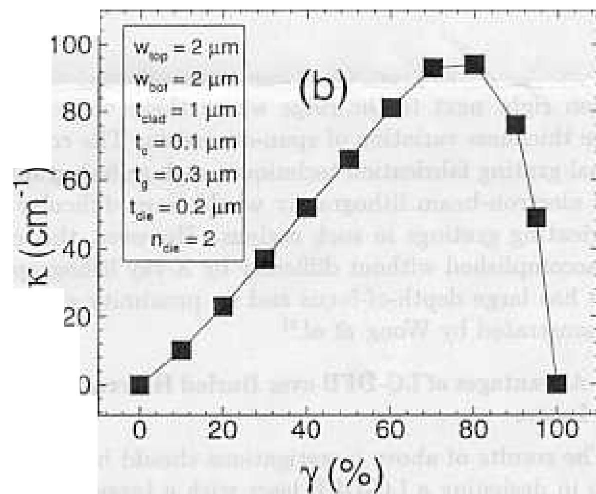

Fig. 6. κ dependence on (a) t_g, grating etching depth, and (b) γ grating duty cycle. γ is larger if less InP is etched away.

t_c and $n_{\rm die}$ respectively. As can be seen, κ decreases as t_c increases since the field decays rapidly in the cladding below the grating region. On the other hand, κ increases only slightly as $n_{\rm die}$ increases. Although larger $n_{\rm die}$ gives slightly larger κ because the field is pulled more into the grating region with larger n_g resulting from larger $n_{\rm die}$ (see eq. (2)), this is a minor effect. The κ dependence on dielectric materials can be ignored for practical purposes given reasonably deep gratings. The values of $n_{\rm die}$ used are selected from three possible dielectric materials: SiO_x with the refractive index of 1.5, polyimide with 1.8, and SiN_x with 2.0.

Three factors related to grating structure are considered: grating etching depth (t_g), the grating duty cycle (γ), and the lateral proximity of gratings to the ridge. Figures 6(a) and 6(b) show the dependence of κ on t_g and γ, respectively. The κ dependence on t_g reveals that κ saturates quickly as t_g increases. This is because the field in the grating region decays quickly with the relatively low value of n_g. From the perspective of κ stability, grating etch depths larger than 0.2 μm should be preferred since then κ is not very sensitive to the variation in t_g. The required gratings have a higher aspect ratio than those in conventional DFB structures, but such gratings can be easily fabricated with dry etching techniques.[15)]

The κ dependence on γ is due to the different field profiles caused by different n_g values resulting from different γ values (see eq. (2)). Although the $\sin(\pi\gamma)$ term in eq. (1) is maximum at $\gamma = 0.5$, Γ becomes larger for larger γ since the field decays less rapidly in the grating region with larger n_g. This strong dependence of κ on the grating duty cycle is a unique feature for the present LC-DFB structure; in conventional DFB structures with buried gratings, there is very little change in Γ as the grating duty cycle changes and the only γ dependence comes from the $\sin(\pi\gamma)$ term.

Figure 7 shows the dependence of κ on the proximity of gratings to the ridge. By this, we are interested in how close gratings are fabricated to the ridge and its influence on κ, as schematically shown in the figure. The figure shows that κ decays rapidly as the grating region moves away laterally from the ridge side-wall. For actual device fabrication, it is then desired that this proximity is well controlled. This is an issue of importance since it is not an easy task to reliably fabricate gratings in the

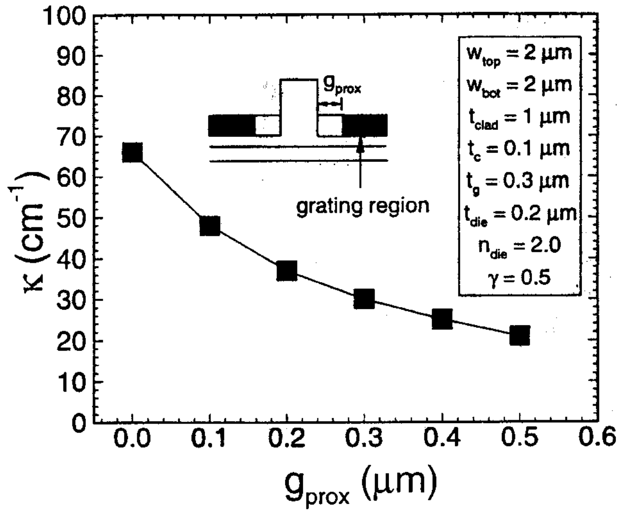

Fig. 7. κ dependence on grating proximity to the ridge, g_{prox}, where the definition of g_{prox} is shown in the figure.

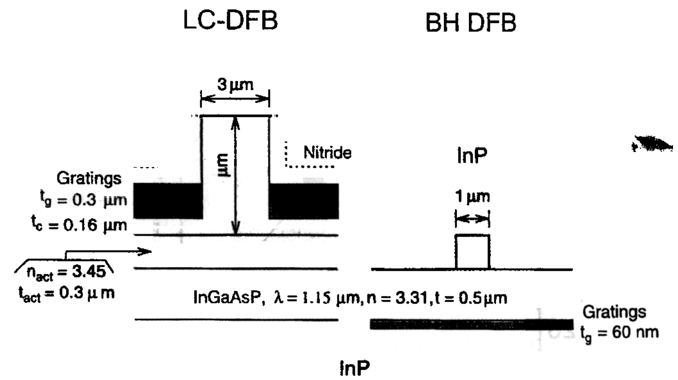

Fig. 8. Schematic drawings of (a) LC-DFB and (b) BH DFB structures used for investigating sensitivities of n_{eff} and λ_{Bragg}.

region right next to the ridge where there will exist a huge thickness variation of spun-on resists. The conventional grating fabrication techniques such as holographic and electron-beam lithography would have difficulty in fabricating gratings in such regions. However, this can be accomplished without difficulty by X-ray lithography that has large depth-of-focus and no proximity effect as demonstrated by Wong *et al.*[2]

5. Advantages of LC-DFB over Buried Heterostructure Lasers

The results of above investigations should be of great help in designing a LC-DFB laser with a target value of κ. Although details of the layer structure given and the ridge and grating structures required by the processing considerations may differ from case to case, the qualitative aspects of κ dependence on parameters investigated above should still hold. With the separation of epitaxial growth and grating fabrication, and the κ tuning capability through straight-forward processing modifications, an approach can be easily envisioned in which one first finds out the qualities of the epitaxially grown laser materials and the characteristics of ridge-waveguide devices without gratings, and designs and fabricates a LC-DFB structure that achieves the required single-mode operation at the target wavelength.

There is an additional advantages of LC-DFB over the conventional buried heterostructure (BH) DFB structures in that the effective mode index, n_{eff}, in LC-DFB is less sensitive to possible processing variations. The processing variation of particular concern here is that occurring during the stripe etching for the active region definition before regrowth in BH and for the ridge formation in LC-DFB devices. Any etching processes have within-the-wafer or wafer-to-wafer nonuniformity, and it is extremely important that a device structure guarantees device parameters that are insensitive to such variations. In order to investigate n_{eff} sensitivities to variations in etched stripe width, the change in n_{eff} of LC-DFB and BH DFB was calculated as a function of the change in etched stripe width. Figure 8 schematically shows LC-DFB and BH DFB structures that are used for this comparison. The device structures are selected so that, first, the resulting κ is about $25\,\mathrm{cm}^{-1}$ as required for practical applications and, second, the stripe width is minimized to suppress higher-order modes. The selected structures were checked not to have any higher-order modes by calculating the allowed propagation constants with the effective index method in which each required effective index is determined by the transfer matrix method. As can be seen in the figure, this results in much narrower active layer width for the BH DFB. For convenience, a BH DFB structure is used in which gratings are fabricated on the substrate. This requires a layer structure with a quaternary layer, whose composition is set to gi the bandgap of 1.15 μm. For a fair comparison, the same layer structure is used for LC-DFB.

The results of this comparison are shown in Figs. 9(a) and 9(b). Figure 9(a) shows the change in κ and (b) in n_{eff} as well as in the Bragg wavelength, λ_{Bragg}. The BH DFB and LC-DFB show comparable sensitivity in κ whose magnitude may not be a great concern, but the change in n_{eff} is much larger for BH DFB. This is a direct result of the fact that the lateral optical confinement inside the buried active region in a BH DFB laser is very strong and a little variation in the active layer width can result in a larger change in the lateral field profile. The facts that BH DFB requires very narrow active width that suffers more from the change in the lateral field profile and that such stripes are usually made with wet-chemical etching, which is more prone to processing variations but minimizes surface damage before regrowth, make the situation worse for BH DFB lasers.

In Fig. 9(b), the change in λ_{Bragg} is directly proportional to that in n_{eff}. This is because λ_{Bragg} in a DFB laser is determined by $\lambda_{\mathrm{Bragg}} = 2 \times n_{\mathrm{eff}} \times \Lambda$, where Λ is the grating period. The change in λ_{Bragg} shown in the figure is calculated by assuming a grating period that gives λ_{Bragg} of 1.55 μm for n_{eff} without any change in stripe width. As can be seen, LC-DFB has very minir change in λ_{Bragg} whereas BH DFB has as much as 20 Å change. Certainly, the yield for desired λ_{Bragg} will be higher for LC-DFB than BH DFB. With this, LC-DFB lasers may turn out to be a not-too-expensive solution for

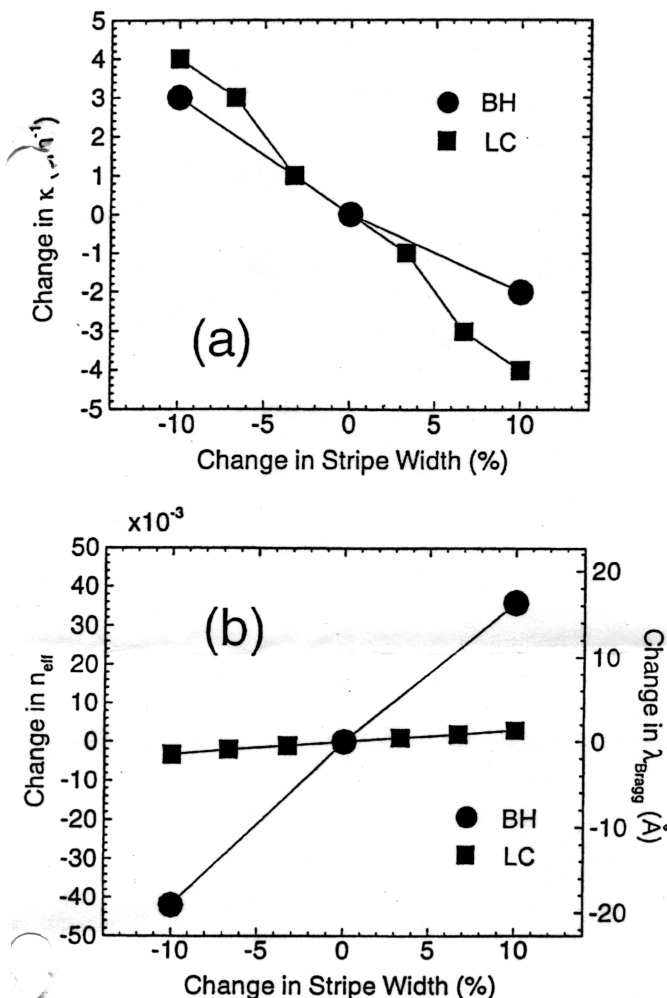

Fig. 9. Changes in (a) κ and n_{eff}, and (b) Bragg wavelength corresponding to stripe width variations.

applications where tight wavelength control is required such as wavelength-division-multiplexing application. It should be noted, however, that the insensitivity of n_{eff} in LC-DFB is due to nature of waveguiding in the ridge waveguide and has nothing to do with the location of gratings, and, consequently, the same advantage should equally apply to conventional ridge-type DFB lasers in which gratings are made on the substrate or buried by re-grown semiconductor.[16)]

6. Conclusion

Results of a systematic study were presented in which dependence of κ on LC-DFB laser structure was investigated. The parameters that were found to have great influence on κ are: ridge width, separation between grating region and active/SCH layers, grating etching depth, grating duty cycle, and grating proximity to the ridge. Careful control of these parameters is required in order to achieve a LC-DFB laser with a targer κ value. In addition, it was shown that LC-DFB lasers are more robust against possible etching process variations and, thus, capable of achieving the target wavelength more reliably than BH DFB lasers.

Acknowledgements

The authors would like to thank Dr. V. V. Wong formerly at MIT but now at SDL for many valuable discussions. We also acknowledge Dr. W. P. Huang and Dr. S. Jüngling for providing portions of the IDBPM code. One of the authors (W. Y. Choi) acknowledges the support of Yonsei University for the present study.

1) L. M. Miller, K. J. Beernink, J. T. Verdeyen, J. J. Coleman, J. S. Hughes, G. M. Smith, J. Honig and T. M. Cockerill: IEEE Photon. Technol. Lett. **4** (1992) 296.
2) V. V. Wong, W.-Y. Choi, J. Carter, C. G. Fonstad and H. I. Smith: J. Vac. Sci. & Technol. B **11** (1993) 2621.
3) R. D. Martin, S. Forouhar, S. Keo, R. J. Lang, R. G. Hunsperger, R. C. Tiberio and P. F. Chapman: IEEE Photon. Technol. Lett. **7** (1995) 244.
4) H. Kogelnik and C. V. Shank: J. Appl. Phys. **43** (1972) 2327.
5) G. P. Agrawal and N. K. Dutta: *Long-Wavelength Semiconductor Lasers* (Van Nostrand Reinhold, New York, 1968) p. 305.
6) J. Hong, W. Huang and T. Makino: J. Lightwave Technol **10** (1992) 1860.
7) D. Yevick and B. Hermansson: Electron. Lett. **21** (1985) 1029.
8) S. Jüngling and J. C. Chen: IEEE J. Quantum Electron. **30** (1994) 2098.
9) K. Handa, S. T. Peng and T. Tamir: Appl. Phys. **5** (1975) 325.
10) G. M. Alman, L. A. Molter, H. Shen and M. Dutta: IEEE J. Quantum Electron. **28** (1992) 650.
11) K. Sato, S. Sekine, Y. Kondo and M. Yamamoto: IEEE J. Quantum Electron. **29** (1993) 1805.
12) W. T. Tsang, F. S. Choa, M. C. Wu, Y. K. Chen and A.M. Sergent: Appl. Phys. Lett. **58** (1991) 2610.
13) C. H. Henry, L. F. Johnson, R. A. Logan and D. P. Clarke: IEEE J. Quantum Electron. **21** (1985) 1887.
14) H. Soda, Y. Kotaki, H. Sudo, H. Ishikawa, S. Yamakoshi and H. Imai: IEEE J. Quantum Electron. **23** (1987) 804.
15) G. J. Van Gurp and J. M. Jacobs: Philips J. Res. **44** (1989) 211.
16) H. Temkin, G. J. Dolan, R. A. Logan, R. F. Kazarinov, N. A. Olsson and C. H. Henry: Appl. Phys. Lett. **46** (1985) 105.